Strong-coupling approach to Mott transition of massless and massive Dirac fermions on honeycomb lattice

Elaheh Adibi[1] and S. Akbar Jafari[1,2,3,*]

[1]*Department of Physics, Sharif University of Technology, Tehran 11155-9161, Iran*

[2]*Center of Excellence for Complex Systems and Condensed Matter (CSCM), Sharif University of Technology, Tehran 1458889694, Iran*

[3]*School of Physics, Institute for Research in Fundamental Sciences, Tehran 19395-5531, Iran*

(Received 30 September 2015; revised manuscript received 13 December 2015; published 10 February 2016)

Phase transitions in the Hubbard model and ionic Hubbard model at half-filling on the honeycomb lattice are investigated in the strong-coupling perturbation theory which corresponds to an expansion in powers of the hopping t around the atomic limit. Within this formulation we find analytic expressions for the single-particle spectrum, whereby the calculation of the insulating gap is reduced to a simple root finding problem. This enables high-precision determination of the insulating gap that does not require any extrapolation procedure. The critical value of Mott transition on the honeycomb lattice is obtained to be $U_c \approx 2.38t$. Studying the ionic Hubbard model at the lowest order, we find two insulating states, one with Mott character at large U and another with single-particle gap character at large ionic potential Δ. The present approach gives a critical gapless state at $U = 2\Delta$ at lowest order. By systematically improving on the perturbation expansion, the density of states around this critical gapless phase reduces.

DOI: 10.1103/PhysRevB.93.075122

I. INTRODUCTION

Graphene is the most extensively studied, both theoretically and experimentally, example of a Dirac solid where the effective motion of charge carriers is described by the Dirac theory in two spatial dimensions. The Dirac theory in graphene is a continuum limit of a simple tight-binding hopping Hamiltonian on a honeycomb lattice of graphene material. Breaking the sublattice symmetry of the underlying honeycomb lattice leads to a mass in the Dirac theory. Such a sublattice symmetry breaking can be either extrinsically induced by the substrate, or intrinsically due to strong Coulomb interactions [1,2]. Recent engineering of the band gap in graphene on SiC brings the study of both massless and massive Dirac fermions into the frontier of graphene research [3]. Therefore, graphene is a natural framework to study both massive and massless Dirac fermions in 2+1 (space+time) dimensions. The atom next to carbon in column IV of the periodic table is Si which also has a two-dimensional allotrope known as silicene with a honeycomb structure, albeit with a larger lattice constant than graphene. Corresponding to larger distance, the hopping amplitude between the neighboring atoms in silicene will be smaller than graphene. Already for the case of graphene, the *ab initio* estimates of the Hubbard U give a value near 10 eV, making a ratio of $U/t \sim 3.3$ [4]. This ratio is even larger in silicene due to larger lattice constant and hence a smaller hopping amplitude. In the case of silicene, the ratio is given by $U/t \approx 4.2$ [5]. Given such large values of U/t in both graphene and silicene where the low-energy effective theory is a Dirac theory, it is necessary to understand the effect of such large values of Hubbard U on the electronic properties of two-dimensional Dirac fermions.

So far, the quantum phase transitions in the honeycomb lattice have been investigated by various theoretical and numerical studies. Sorella *et al.* methods the half-filled Hubbard model on graphene's honeycomab lattice using quantum Monte Carlo (QMC) simulations which found critical interaction $U_c/t = 4.5 \pm 0.5$ for semimetal to antiferromagnetic phase transition [6]. Herbut within renormalization group (RG) in the large-N limit showed that the semimetal to Mott insulator transition (SMIT) occurs at a finite U/t value for the physical case $N = 2$ [7]. Using functional RG in Ref. [8], the critical minimal interaction strength toward antiferromagnetic instability is found to be $U_c/t = 3.8$. The Mott transition has been studied by dynamical mean field theory (DMFT) calculations where the SMIT is shown to occur at relatively large interaction strength $U_c > 10t$ [9,10]. The DMFT estimate of critical interaction is improved by performing cluster dynamical mean field theory (CDMFT) to $U_c/t = 3.3$ [11], $U_c/t = 3.7$ [12], and $U_c/t = 3$–4 [13]. The above difference between the DMFT and CDMFT results is due to the fact that honeycomb lattice is a two-dimensional lattice with the smallest coordination number, so CDMFT includes the spatial correlations missed in DMFT. The Mott transition on the honeycomb lattice was also investigated within slave-particle technique by Vaezi *et al.* who obtained a critical interaction $U_c \simeq 3t$ [14]. The possible existence of a spin liquid phase on the honeycomb lattice investigated by Meng *et al.* using large-scale QMC calculations for clusters containing up to 648 sites. Their putative quantum spin liquid phase was found for the range $U = 3.5t$ to $U_{\rm AF} = 4.3t$ [15]. The presence of spin liquid phase has been supported by other studies based on variational cluster approximation [16], CDMFT [17], and density matrix embedding theory [18]. The spin liquid phase has been challenged by Sorella *et al.* who performed the same QMC calculations as in Meng *et al.* for larger clusters including up to 2592 sites and found a direct SMIT at $U_{\rm AF}/t = 3.869 \pm 0.013$ [19]. Moreover, recent studies have indicated that existence of spin liquid phase is rather implausible and have also confirmed a continuous transition from semimetal to Mott (antiferromagnetic) insulator at critical interaction $U_c/t = 3.8 \pm 0.1$ [20–23].

*akbar.jafari@gmail.com

Motivated by the above discussions, we investigate the phase transition from the Mott side. A natural framework to approach from the infinite-U side is strong-coupling perturbation theory to expand in powers of t/U. This can be done in two ways: (1) the first choice is to do brute force perturbation theory [24], or (2) the other way is to use a dual transformation and to rewrite the strongly correlated Hamiltonian in terms of dual degrees of freedom [25]. We find the latter approach rewarding as it clearly indicates the onset of gap closing by approaching from the strong-coupling side. Despite some pathologies in the analytic continuation, in the lower orders of perturbation theory considered here, we are able to obtain closed-form formulas for the spectral functions without encountering the problems of analytic continuation faced by earlier investigators [25,26]. Within this approach we identify the Mott transition in the half-filled massless Dirac sea at zero temperature. Given our analytic formulas for the spectral functions, the determination of Mott gap is reduced to a simple root finding problem that can be done with arbitrary precision. This does not require extrapolation procedure [20,27–29]. Approaching from the Mott side, one might think that electrons being localized in the Mott phase do not have any idea what is going to happen when the Hubbard U is reduced. However, on the weak-coupling side we know that the underlying honeycomb structure leads to Dirac spectrum. Therefore, the question would be how does the Mott phase know that upon reducing the Hubbard U it should become a Dirac solid? An interesting picture that emerges within the present dual transformation approach is that deep in the Mott phase, the dual fermions have a Dirac cone structure, albeit far away from the Fermi level within the high-energy states of upper and lower Hubbard bands, and hence the Dirac "genome" is passed across the quantum critical point separating the Dirac liquid and the Mott insulating phase.

We also take the same approach to study the massive Dirac fermions approaching from the Mott side. For this model, the U/t is not the only parameter governing the phase diagram. The presence of another energy scale Δ related to gap (mass) makes it more complicated. In the large-U limit again we have the Mott phase. When the Hubbard U is negligible in comparison to Δ, its main effect is to renormalize Fermi liquid parameters of the underlying metallic state, and hence the relevant parameter Δ opens up a single-particle gap and we have a band insulator [30]. For the intermediate regime, our earlier DMFT study suggests the presence of a gapless semimetallic state which is born out of the competition between the two parameters U and Δ [31,32]. Within the present approach at the lowest orders of the kinetic energy t, we find that there is a critical point separating the Mott and band insulating phases. The system at this critical point is gapless and corresponds to a semimetallic (Dirac cone) state. Systematically improving the perturbation theory by going to higher orders shows that the density of states (DOS) around this quantum critical semimetallic states tends to deplete.

The paper is organized as follows. We begin by reviewing the strong-coupling expansion method in Sec. II. In Sec. III, the method is applied to the half-filled Hubbard model and by using an analytic approach the critical interaction of the Mott transition is obtained. The method is also employed to investigate the possible phases of the half-filled ionic Hubbard model in Sec. IV. Finally, our findings are summarized and conclusions are drawn in Sec. V. The paper is accompanied by two appendixes which present the expression for DOS on honeycomb lattice and our formulas for self-energies of auxiliary fermions in the ionic Hubbard model case.

II. METHOD OF CALCULATION

We employ the strong-coupling expansion to study SMIT of the Hubbard model on the honeycomb lattice. We also use this method to characterize phase diagram of the ionic Hubbard model at zero temperature. In what follows, we briefly describe the method proposed in Ref. [25]. Generally speaking, in the strong-coupling limit, the Hamiltonian is written as the sum of the unperturbed local Hamiltonian H_0 and the perturbation H_1:

$$H = H_0 + H_1. \tag{1}$$

According to formulation of Ref. [25], $H_0 = \sum_i h_i(c^\dagger_{i\sigma}, c_{i\sigma})$ where H_0 is diagonal in variable i and σ denotes all the other variables of the problem. If we assume i as site variable, H_0 is written as a sum over onsite Hamiltonians h_i. On the other hand, H_1 is supposed to be a one-body hopping operator $H_1 = \sum_{ij}\sum_\sigma V_{ij} c^\dagger_{i\sigma} c_{j\sigma}$ where the Hermitian matrix V is the hopping amplitude between orbitals located at sites i, j. The partition function in the path-integral formulation can then be expressed as

$$Z = \int [d\gamma^\star\, d\gamma]\, \exp\Bigg[-\int_0^\beta d\tau \Bigg\{ \sum_{i\sigma} \gamma^\star_{i\sigma}(\tau)(\partial_\tau - \mu)\gamma_{i\sigma}(\tau) + \sum_i h_i(\gamma^\star_{i\sigma}(\tau), \gamma_{i\sigma}(\tau)) + \sum_{ij\sigma} \gamma^\star_{i\sigma}(\tau) V_{ij} \gamma_{j\sigma}(\tau) \Bigg\} \Bigg], \tag{2}$$

where $\gamma_{i\sigma}(\tau)$, $\gamma^\star_{i\sigma}(\tau)$ denote Grassmann fields of the electrons and β is inverse of temperature T. In the Hubbard-type models H_0 is not quadratic, hence the simple form of an ordinary Wick theorem can not be used to construct a diagrammatic expansion for the Green's functions.[1] Introducing the auxiliary Grassmann fields $\psi_{i\sigma}(\tau)$, $\psi^\star_{i\sigma}(\tau)$ via the Grassmann version of the Hubbard-Stratonovich transformation [33] we can write

$$\begin{aligned} &\int [d\psi^\star d\psi] \exp\Bigg[\int_0^\beta d\tau \sum_{i\sigma} \Bigg\{ \sum_j \psi^\star_{i\sigma}(\tau)(V^{-1})_{ij}\psi_{j\sigma}(\tau) \\ &\qquad + \psi^\star_{i\sigma}(\tau)\gamma_{i\sigma}(\tau) + \gamma^\star_{i\sigma}(\tau)\psi_{i\sigma}(\tau) \Bigg\} \Bigg] \\ &= \det(V^{-1}) \exp\Bigg[-\int_0^\beta d\tau \sum_{ij\sigma} \gamma^\star_{i\sigma}(\tau) V_{ij} \gamma_{j\sigma}(\tau) \Bigg]. \end{aligned} \tag{3}$$

With the aid of this equation, the the partition function can be rewritten as

$$Z = \int [d\psi^\star d\psi] \exp\Bigg[-\Bigg\{ S_0[\psi^\star, \psi] + \sum_{R=1}^{\infty} S^R_{\rm int}[\psi^\star, \psi] \Bigg\} \Bigg], \tag{4}$$

[1] Although a more complicated version of the Wick theorem still exists, it is not easy or intuitive to work with.

where the action has a free auxiliary fermion part given by the inverse of the hopping matrix of original fermions

$$S_0[\psi^\star,\psi] = -\int_0^\beta d\tau \sum_{ij\sigma} \psi^\star_{i\sigma}(\tau)\,(V^{-1})_{ij}\,\psi_{j\sigma}(\tau), \quad (5)$$

and an infinite number of interaction terms

$$S^R_{\rm int}[\psi^\star,\psi] = \frac{-1}{(R!)^2}\sum_i \sum_{\{\sigma_l\sigma'_l\}} \int_0^\beta \prod_{l=1}^R d\tau_l d\tau'_l \times \psi^\star_{i\sigma_1}(\tau_1)\ldots\psi^\star_{i\sigma_R}(\tau_R)\psi_{i\sigma'_R}(\tau'_R)\ldots\psi_{i\sigma'_1}(\tau'_1) \times\left\langle\gamma_{i\sigma_1}(\tau_1)\ldots\gamma_{i\sigma_R}(\tau_R)\gamma^\star_{i\sigma'_R}(\tau'_R)\ldots\gamma^\star_{i\sigma'_1}(\tau'_1)\right\rangle_{0,c}. \quad (6)$$

The above equation denotes a vertex with R incoming ψ fermions and R outgoing ψ fermions. Note again that ψ fermions are auxiliary (dual) fermions. Thinking in terms of ψ fermions, now their kinetic energy scale is given by V^{-1} which is a large number when the kinetic energy V of the original fermions is much smaller than the Coulomb energy scale U. Therefore, standard diagrammatic perturbation theory can be applied. The only (very important) difference with the textbook diagrammatics will be that in the present case the vertex is not a simple number, but acquires a nontrivial dynamical structure given by the the cumulant average $\langle\ldots\rangle_{0,c}$ of the original Grassmann fields. These are the connected correlation functions of original fermions with respect to the local Hamiltonian h_i. Higher-order cumulants are expected to be less important in the limit of large U. Lower-order cumulants which only depend on the form of the local Hamiltonian h_i, can be calculated straightforwardly [34]. Once the multiparticle cumulants of the original fermions are known, they act as dynamic vertices for the auxiliary fermions and from this point, we can use standard perturbation theory for the auxiliary fields. Eventually, if G denotes the Green's function of the original fermions and Γ the self-energy of the auxiliary fermions, the relation between them is given by [26]

$$G = (\Gamma^{-1} - V)^{-1}. \quad (7)$$

This means to obtain Green's function, we have to compute the self-energy Γ of the auxiliary fermions which can be done with standard perturbation theory. Further details of the method are given in Refs. [25,26] and will not be repeated here.

In the following sections, we apply the method presented here to two models at half-filling on the honeycomb lattice, namely, the Hubbard model and ionic Hubbard model. On the honeycomb lattice, free propagator of the auxiliary fermions is determined by

$$V(\mathbf{k}) = \begin{pmatrix} 0 & ts(\mathbf{k}) \\ ts^\star(\mathbf{k}) & 0 \end{pmatrix}, \quad (8)$$

where $\mathbf{k} = (k_x,k_y)$, and $s(\mathbf{k}) = \exp(-ik_x a) + 2\exp(\frac{ik_x a}{2})\cos(\frac{\sqrt{3}k_y a}{2})$. The atomic separation of the honeycomb lattice assumed to be $a = 1$. The 2×2 matrix structure comes from the two-sublattice structure of the honeycomb lattice. In the following, we use the standard perturbation theory to study the Hubbard and ionic Hubbard models the noninteracting limit of which corresponds to massless and massive Dirac fermions.

III. HUBBARD MODEL

The Hubbard Hamiltonian for spin-$\frac{1}{2}$ fermions is given by

$$H = -t\sum_{\langle ij\rangle,\sigma}(c^\dagger_{i\sigma}c_{j\sigma} + \text{H.c}) + U\sum_i n_{i\uparrow}n_{i\downarrow} - \mu\sum_{i\sigma} n_{i\sigma}, \quad (9)$$

where $c^\dagger_{i\sigma}$ ($c_{i\sigma}$) creates (annihilates) a fermion of spin projection $\sigma = \uparrow, \downarrow$ on lattice site i, $n_{i\sigma} = c^\dagger_{i\sigma}c_{i\sigma}$, t denotes the nearest-neighbor hopping amplitude, and $U \geqslant 0$ denotes the strength of the onsite repulsion. Through the paper, we focus at half-filling ($\sum_\sigma\langle n_{i\sigma}\rangle = 1$) by setting the chemical potential μ to $U/2$. For the strong-coupling expansion of the Hubbard model, H_0 corresponds to the atomic limit and H_1 is equivalent to the kinetic term. The diagrams contributing to Γ up to order t^2 are presented in Fig. 1, which lead to the following expression for Γ [26]:

$$\Gamma(i\omega) = \left(\frac{i\omega}{(i\omega)^2 - (U/2)^2} + \frac{3.45\,t^2(U/2)^2(i\omega)}{[(i\omega)^2 - (U/2)^2]^3}\right)\mathbb{I}, \quad (10)$$

where $i\omega$ denotes a complex frequency and $\mathbb{I}$ stands for 2×2 identity matrix in the space of two sublattices.

As is evident from the above self-energy (for more details see Ref. [25]), the above self-energy violates the causality. A causal Green's function (or self-energy) is Lehmann representable if it can be written as a Jacobi continued fraction form. So one has to find out a Jacobi continued fraction form of self-energy Eq. (10) which in this case is simple and turns out to be

$$\Gamma(i\omega) = \cfrac{1}{i\omega - \cfrac{(U/2)^2}{i\omega - \cfrac{3.45\,t^2}{i\omega - \cfrac{(U/2)^2}{i\omega}}}}\,\mathbb{I} \quad (11)$$

which is equivalent to Eq. (10) up to $(t/U)^2$. Now we can calculate the Green's function by substituting self-energy into Eq. (7). In order to monitor the Mott transition, we should calculate the DOS $\rho(\omega) = -\frac{1}{\pi}\lim_{\eta\to 0^+}\sum_{\mathbf{k}}\text{Im Tr } G(\mathbf{k},\omega + i\eta)$ at different interaction strength. In other words, to identify the electronic properties of the system by increasing U, we calculate the single-particle gap that extracted from DOS by integration over wave vectors numerically. But, in doing so, it is hard to judge when the gap opens by increasing U due to artificial Lorentzian broadening η used in the Greens' functions to avoid numerical divergences. As we will explain shortly in the following, we are able to work out the integration analytically which enables us to avoid both numerical errors

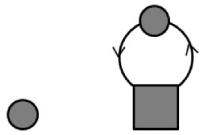

FIG. 1. Diagrams contributing to the self-energy of the auxiliary fermions up to order t^2 where solid lines indicate free propagator V of auxiliary fermions and vertices represent connected correlation functions. Circles are one-particle connected correlation functions and squares refer to two-particle connected correlation function.

as well as the continued fraction issues. This reduces the determination of the Mott gap into a simple root finding problem which can be solved with arbitrary precision.

Assuming the self-energy of auxiliary fermions in Eq. (10) [or Eq. (11)] has a more general form $\Gamma = \mathcal{F}(i\omega)\mathbb{I}$ and plugging in Eq. (7), the DOS of physical electrons is given by

$$\rho(\omega) = -\frac{1}{\pi}\lim_{\eta\to 0^+}\sum_{\mathbf{k}}\mathrm{Im}\Bigg[\frac{1}{1/\mathcal{F}(\omega+i\eta)-t|s(\mathbf{k})|} + \frac{1}{1/\mathcal{F}(\omega+i\eta)+t|s(\mathbf{k})|}\Bigg]. \tag{12}$$

On the other hand, in the noninteracting honeycomb lattice (graphene), the DOS of a hopping Hamiltonian is given by [35]

$$\rho_0(\omega) = -\frac{1}{\pi}\lim_{\eta\to 0^+}\sum_{\mathbf{k}}\mathrm{Im}\Bigg[\frac{1}{\omega+i\eta-t|s(\mathbf{k})|} + \frac{1}{\omega+i\eta+t|s(\mathbf{k})|}\Bigg] = \frac{|\omega|}{\pi^2}\frac{1}{\sqrt{Z_0}}K\left(\sqrt{\frac{Z_1}{Z_0}}\right), \tag{13}$$

where

$$Z_0 = \begin{cases}(1+|\omega|)^2-(\omega^2-1)^2/4, & |\omega|<1\\ 4|\omega|, & 1\leqslant|\omega|\leqslant 3\end{cases} \tag{14}$$

and

$$Z_1 = \begin{cases}4|\omega|, & |\omega|<1\\ (1+|\omega|)^2-(\omega^2-1)^2/4, & 1\leqslant|\omega|\leqslant 3.\end{cases} \tag{15}$$

Here, $K(x)$ is the complete elliptic integral of the first kind [36]. This representation is valid as long as the imaginary part of the argument passed into the above function is negligible. By comparison of Eqs. (12) and (13), the DOS of interacting problem is analytically obtained as

$$\rho(\omega) = \rho_0[\mathcal{F}^{-1}(\omega)]. \tag{16}$$

This representation is valid as long as $\mathcal{F}^{-1}$ has a negligible imaginary part. For the pure Hubbard model it turns out that when $\mathcal{F}^{-1}$ is evaluated at $\omega+i0^+$, its imaginary part tends to zero. Therefore, the above representation is valid. A nice property of the function ρ_0 is that it vanishes when its argument $|\omega|$ exceeds 3. This statement is exact and involves no numerical errors. Therefore, for the pure Hubbard model, the gap opening corresponds to the condition

$$|\mathcal{F}^{-1}(\omega+i0^+)|>3. \tag{17}$$

Based on particle-hole symmetry, we expect the Mott-Hubbard gap to open up at $\omega=0$, we only need to monitor the behavior of $\mathcal{F}^{-1}$ at $\omega=0$. When this quantity is larger than 3, the DOS is zero, and hence we have a gap. Therefore, starting from the large-U side it only suffices to monitor the function $\mathcal{F}^{-1}$ at $\omega=0$ for various values of U. Upon reducing U, once this value drops below 3 indicates that we have entered the conducting phase. Therefore, we have reduced the problem of determination of the Mott gap into a root finding problem defined by Eq. (17) which can be solved with arbitrary precision at negligible computational cost. In this work, we determine the gaps up to the precision of $10^{-4}t$. Note that within the methods based on Jacobi continued fraction followed by numerical integration scarcely can get such resolutions.

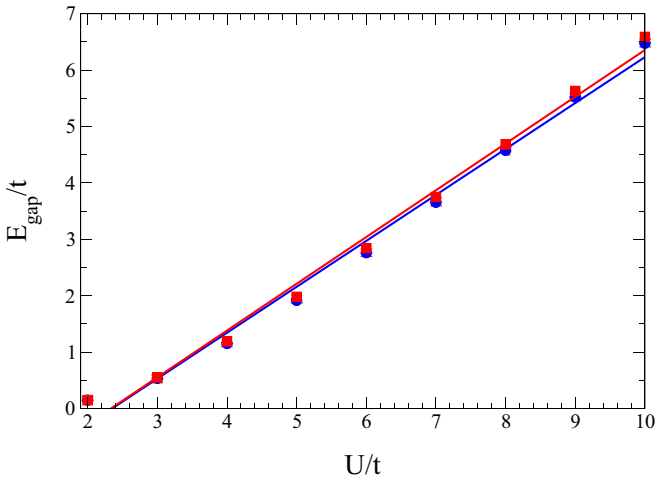

FIG. 2. U dependence of the single-particle gap calculated from Eq. (17). For the self-energy $\mathcal{F}(\omega+i0^+)$ we can use both Eqs. (10) (red squares) and (11) (blue circles). The red (blue) line indicates the best *linear* fit to red (blue) data.

Let us now implement condition (17) to study the Mott transition on the honeycomb lattice. In Fig. 2, the single-particle gap E_{gap} as extracted from Eq. (17) versus onsite interaction U is shown. As we study the Mott transition from strong-coupling limit, the single-particle gap is determined for large interaction strengths from the behavior of $\mathcal{F}(\omega)$, i.e., the self-energy of auxiliary fermions. Now, to evaluate this self-energy, we have two options: one is to use Eq. (10) and the other is to use the continued fraction form (11). Note that these options are not available in the absence of analytic formula for DOS. As can be seen in Fig. 2, the two procedures agree on the value of Hubbard gap obtained from the condition (17). To characterize the critical Coulomb interaction U_c for the SMIT, we do not bother with extrapolations of the Lorentzian width of the numerical integration as the limit $\eta\to 0$ has been properly encoded in Eq. (13). We approach from the Mott side where we are sure that (1) the method is more reliable as it is a perturbation from the Mott side, and (2) the gap is clearly open. Then, having a number of data in the Mott side, we extrapolate by fitting the data to find out the value of U at which E_{gap} extrapolates to zero. With this approach we find $U_c = 2.38t$ for the Mott transition within the present second-order strong-coupling approximation. Our motivation to use a linear fit is that in the atomic limit the upper and lower Hubbard bands are expected to behave linearly with U, and the present method as well builds on the atomic limit within the auxiliary fermions method.

In recent years, the critical exponent characterizing the Mott criticality has been of interest [19,23,37–39]. Trying to fit a nonlinear function of the form $E_{\mathrm{gap}}\propto(U-U_c^{\mathrm{nonlin}})^{\beta_g}$ to the same set of data represented in Fig. 2, we obtain

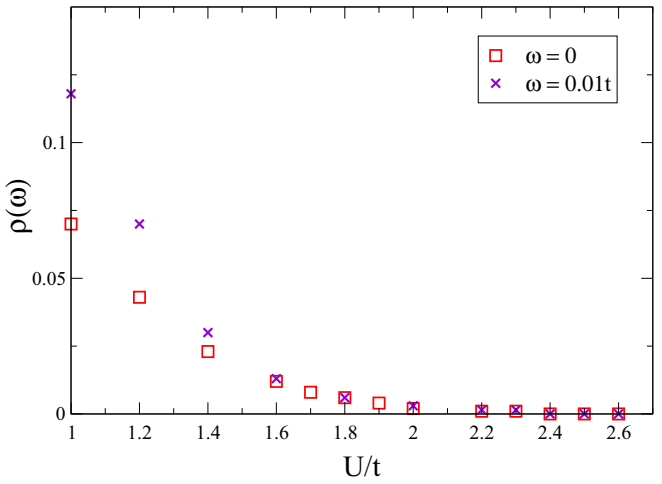

FIG. 3. The $\eta \to 0$ extrapolated $\rho(\omega)$ for $\omega = 0$ and $0.01t$ as a function of the onsite Coulomb interaction U on the honeycomb lattice.

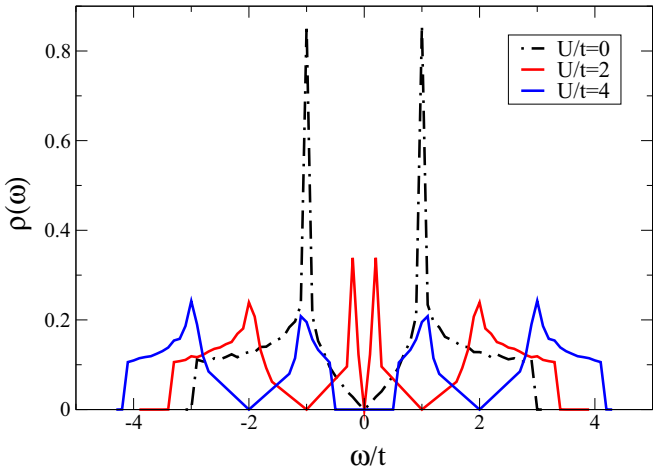

FIG. 4. DOS of the Hubbard model on honeycomb lattice. DOS at $U = 0$ is given for reference.

the gap exponent as $\beta_g = 1.28 \pm 0.04$ and the critical value corresponding to nonlinear fit $U_c^{\text{nonlin}} = 1.75 \pm 0.13$. But, since our method and data are reliable for values of U deep in the Mott phase, we reckon that the linear fit is more consistent with the method used to extract the gap data. As will be explained in the sequel, using other diagnostic tools we also get a value for U_c which is close to 2.38 found from the above linear fit.

To demonstrate the advantage of the present analytical approach, let us see how the previous authors [20,27–29] find out the onset of gap formation. First, for a small but finite value of η, the integral required in Eq. (12) is calculated by numerical integration over wave vectors of the first Brillouin zone of the honeycomb lattice. Thus, one computes $\rho^{\eta}(\omega)$ for a few values of the Lorentzian broadening parameters η at $\omega = 0$. Then, by means of polynomial fitting one extrapolates to the $\eta \to 0$ limit. The extrapolated $\rho(\omega = 0)$ must vanish in the insulating phase. However, this is ambiguous because even in the Dirac (non-Mott) phase the DOS at $\omega = 0$ is expected to be zero. To somehow get around this, it was suggested to focus on the DOS at slightly different energy scale, e.g., $\omega = 0.01t$ [20]. We have presented a comparison of these two in Fig. 3. This figure suggests that the Mott phase is stabilized for $U \geqslant 2.4t$. However, the nonzero DOS at $\omega = 0$ in the semimetallic side is not remedied. As advertised, the critical value of 2.4 obtained in this way is very close to our linear fit value of $U_c = 2.38$, and hence we maintain that the linear fit is better suited for the data obtained from the present method.

Now, let us employ the present analytical formula to study the profile of the DOS as a function of the Hubbard U. In Fig. 4 we plot DOS obtained from Eq. (16). The noninteracting DOS has been denoted by dotted line for reference. As can be seen in the semimetallic phase, there is a linear DOS feature at $\omega = 0$ which is due to the Dirac cone at the K points of the Brillouin zone. But in addition, there appears another valley in DOS which would correspond to Dirac cone at higher-energy scales corresponding to $\omega = U/2$. Interestingly, this feature survives in the Mott phases where the major low-energy Dirac cone has been gapped out by strong U. This can be easily understood from the form of Eq. (10): As can be seen, the auxiliary fermion self-energy Γ diverges at $\omega = \pm U/2$, which corresponds to $\mathcal{F}^{-1} = 0$. But from Eq. (16), when the argument of bare ρ_0 becomes zero, it will correspond to a Dirac node. This feature may help to shed light on the meaning of auxiliary fermions: the divergence in the self-energy of auxiliary fermions corresponds to Dirac nodes of the original electrons.

At this point, let us emphasize that *the expression of DOS in terms of a function $\mathcal{F}$ is quite general*. This is because the expansion is basically in powers of the hopping matrix $V(\mathbf{k})$ which is a combination of Pauli matrices. But, since odd powers of the Pauli matrices do not survive the trace, only even powers corresponding to even orders of perturbation expansion survive the trace needed in calculation of DOS. Therefore, at any (even) order of perturbation theory, DOS can be expressed in the form of Eq. (16). Going to higher orders only improves the dynamical structure of the function $\mathcal{F}(\omega)$.

IV. IONIC HUBBARD MODEL

Now that we are equipped with Eq. (16) to analytically obtain DOS within a given order of strong-coupling perturbation theory, and we have checked that it gives reasonable results for the case of Mott transition in the Hubbard model, let us break the sublattice symmetry by adding a scalar potential $\pm\Delta$ to the two sublattices. This potential is known as ionic potential and hence the Hamiltonian of the ionic Hubbard model is given by

$$H = -t \sum_{\substack{i\in A, j\in B,\\ \sigma}} (c_{i\sigma}^{\dagger} c_{j\sigma} + \text{H.c.}) + U \sum_{i} n_{i\uparrow} n_{i\downarrow} + \Delta \sum_{i\in A,\sigma} n_{i\sigma} - \Delta \sum_{j\in B,\sigma} n_{i\sigma} - \mu \sum_{i\sigma} n_{i\sigma}. \quad (18)$$

In the atomic limit ($t = 0$), the model reduces to classical Ising-type effective model that contains various insulating phases [31]. At the simplest level, setting $t = 0$ in the above Hamiltonian and corresponding to half-filling, the essential competition is between Δ and U terms. When the ionic

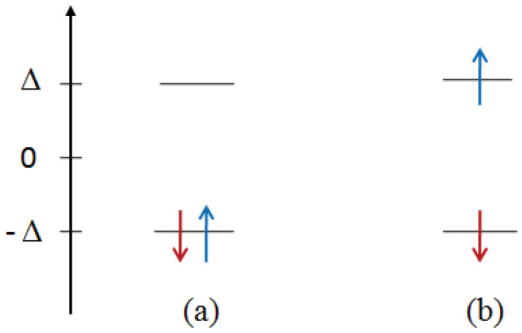

FIG. 5. Atomic limit schematic representation of (a) $U < 2\Delta$ and (b) $U > 2\Delta$.

potential dominates, i.e., $\Delta \gg U$ as can be seen in the left part of the schematic drawing of Fig. 5, both up- and down-spin electrons are pilled in a sublattice whose ionic potential is lower. In this limit, the U is not enough to exclude the double occupancy. However, in the opposite limit of $U \gg \Delta$, the double occupancy is excluded and the system becomes a Mott insulator with a charge gap $\sim U$. Then, the important question is what is the nature of the ground state for the $U \sim \Delta$ regime when the fluctuations arising from the kinetic term (t) are turned on?

Tackling the problem with strong-coupling perturbation theory, in this case the H_0 part of the Hamiltonian will contain only U and Δ terms and the perturbation term H_1 will be the hopping term. Therefore, we expect the method to be reliable only when both Δ and U are quite larger than the hopping t. But, even in the limit $U, \Delta \gg t$, it is interesting to have an idea of the nature of the gap when U and Δ are comparable.

Now, the H_0 part not only contains the parameter U, but also contains the energy scale Δ. Therefore, the corresponding vertices of the auxiliary fermions have a built-in structure containing the competition between U and Δ. The role of ionic Δ can be easily incorporated as two different types of chemical potential for the two sublattices. If we denote the self-energy of the auxiliary fermions on sublattices A and B with $\Gamma^{(A)}$ and $\Gamma^{(B)}$, respectively, we obtain the self-energy of auxiliary fermions on the lattice as

$$\Gamma(i\omega) = \begin{pmatrix} \Gamma^{(A)}(i\omega) & 0 \\ 0 & \Gamma^{(B)}(i\omega) \end{pmatrix}, \tag{19}$$

and the DOS is given by

$$\rho(\omega) = -\frac{1}{\pi}\frac{1}{2}\left(\sqrt{\frac{\Gamma^{(A)}(\omega)}{\Gamma^{(B)}(\omega)}} + \sqrt{\frac{\Gamma^{(B)}(\omega)}{\Gamma^{(A)}(\omega)}}\right) \times \lim_{\eta\to 0^+}\sum_{\mathbf{k}} \mathrm{Im}\left[\left(\frac{1}{\frac{1}{\sqrt{\Gamma^{(A)}(\omega+i\eta)\Gamma^{(B)}(\omega+i\eta)}} - t|s(\mathbf{k})|} + \frac{1}{\frac{1}{\sqrt{\Gamma^{(A)}(\omega+i\eta)\Gamma^{(B)}(\omega+i\eta)}} + t|s(\mathbf{k})|}\right)\right]. \tag{20}$$

Comparison between Eqs. (20) and (13) leads to the following expression for DOS:

$$\rho(\omega) = \frac{1}{2}\left(\sqrt{\frac{\Gamma^{(A)}(\omega)}{\Gamma^{(B)}(\omega)}} + \sqrt{\frac{\Gamma^{(B)}(\omega)}{\Gamma^{(A)}(\omega)}}\right)\rho_0\left(\mathcal{F}_1^{-1}\right), \tag{21}$$

with

$$\mathcal{F}_1 = \sqrt{\Gamma^{(A)}(\omega)\Gamma^{(B)}(\omega)}. \tag{22}$$

The representation (21) is valid as long as the function $\mathcal{F}_1$ is purely real. In the case of ionic Hubbard model, the above function when evaluated at $\omega + i0^+$ is either purely real, which makes the above representation reliable, or purely imaginary. In the latter case, a more general formula for the Green's function of hopping Hamiltonians derived by Horiguchi [40] must be used. This has been summarized in Appendix A. The expression of Horiguchi is valid for any complex argument. Evaluation of the resulting DOS for purely imaginary arguments shows that it becomes identically zero. Therefore, the insulating gap is determined by

$$\left|\mathcal{F}_1^{-1}(0)\right| > 3 \quad \text{or} \quad \mathrm{Re}[\mathcal{F}_1(0)] = 0. \tag{23}$$

Note again that, so far we have not specified the self-energy matrix elements $\Gamma^{(A)}$ and $\Gamma^{(B)}$ and, therefore, the discussion up to now remains quite general. Depending on the order of perturbation theory, these quantities may have different expressions. But, the important point is that their dynamical structure, as well as their parametric dependence on U and Δ contains the essential physics of the interplay between the Mott insulating phase and band insulating phase. As before, the energy-dependent quantity $\mathcal{F}_1$ determines the gap opening as well as the formation of Dirac nodes in the system.

Let us proceed with our discussion of the ionic Hubbard model by defining the mean occupation for a given spin projection on each sublattice at half-filling,

$$n^{(A)} = \frac{e^{\beta(u-\Delta)} + e^{-2\beta\Delta}}{1 + 2e^{\beta(u-\Delta)} + e^{-2\beta\Delta}},$$
$$n^{(B)} = \frac{e^{\beta(u+\Delta)} + e^{2\beta\Delta}}{1 + 2e^{\beta(u+\Delta)} + e^{2\beta\Delta}}, \tag{24}$$

where for brevity we have used u for $U/2$. Note that in the case of simple Hubbard model where $\Delta = 0$, the zero-temperature limit ($\beta \to \infty$) gives a very simple result $n^{(A)} = n^{(B)} = \frac{1}{2}$ for each spin projection.

A. Zeroth order

Now, let us start by the lowest order of the perturbation theory for the ionic Hubbard model. Keeping only zeroth-order diagram in powers of t depicted in Fig. 1, the self-energies of the auxiliary fermions on two sublattices become

$$\Gamma^{(A)}(i\omega) = \frac{1 - n^{(A)}}{i\omega + U/2 - \Delta} + \frac{n^{(A)}}{i\omega - U/2 - \Delta}, \tag{25}$$
$$\Gamma^{(B)}(i\omega) = \frac{1 - n^{(B)}}{i\omega + U/2 + \Delta} + \frac{n^{(B)}}{i\omega - U/2 + \Delta}. \tag{26}$$

Let us first employ Eq. (21) to generate a plot of DOS. As pointed out, the present approach being a strong-coupling expansion is reliable when $U, \Delta \gg t$. In generating the plots

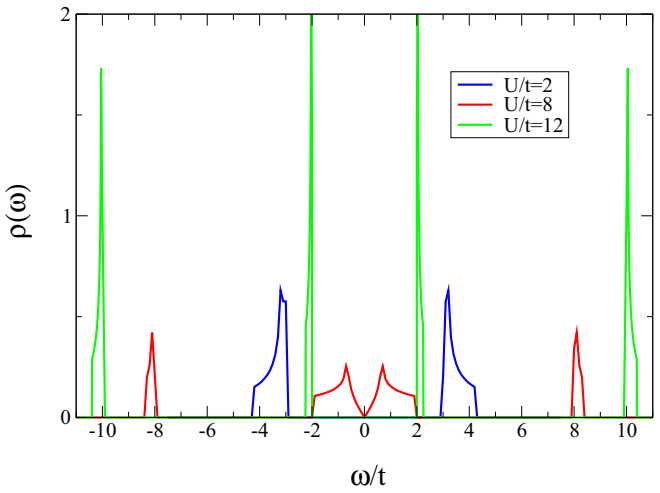

FIG. 6. DOS of the zeroth-order diagram for $\Delta = 4t$ in half-filled ionic Hubbard model on honeycomb lattice at zero temperature. The different colors as indicated in the legend correspond to band insulating state ($U = \Delta/2$), semimetallic state ($U = 2\Delta$), and Mott insulating state ($U = 3\Delta$).

we set $\Delta = 4t$ and $T = 0$. As can be seen in Fig. 6, we have three different situations. The blue plot corresponds to $U = 2t = \Delta/2$ where there is a gap in the spectrum, and there are no signatures of upper and lower Hubbard bands. In this case, the gap is dominated by a single-particle character coming from the ionic potential Δ. By increasing U, we get to the red plot that corresponds to $U = 8t = 2\Delta$. There is a very beautiful linear V-shaped pseudogap in the spectrum characteristic of a Dirac cone in two dimensions. At the same time, there are also signatures of upper and lower Hubbard band formation at higher-energy scales. Upon further increase of the Hubbard parameter for $U = 12t = 3\Delta$ (green plot), again a gap opens up on top of a Dirac liquid state [9]. This gap has a Mott nature and features of upper and lower Hubbard bands are visible. In Table I, we have extracted the precise gap values from the criteria on $\mathcal{F}_1^{-1}$ [Eq. (23)].

Therefore, the essential physics emerging here is that the competition between two gapped states at $U \gg \Delta$ (Mott state) and $U \ll \Delta$ (band insulating state) gives rise to a conducting state which in this case is a Dirac liquid state. This is in agreement with our previous DMFT finding [32]. However, note that within the DMFT we find a conducting (Dirac) *region* sandwiched between the Mott and band insulating phases, while in the present strong-coupling expansion the ensuing conducting (Dirac) state at the lowest order is a quantum critical Dirac state. Indeed, the existence of a Dirac cone at $U = 2\Delta$ can be seen analytically from the lowest-order expressions (25) and (26). Let us first take the limit $T \to 0$ or equivalently $\beta \to \infty$. In this limit, one has $n^{(A)} = \frac{1}{3}$ and $n^{(B)} = \frac{2}{3}$ when both $U, \Delta > 0$. Flipping the sign of Δ amounts to swapping the occupancies of the two sublattices. In this limit, the self-energies of the two sublattices will become

$$\Gamma^{(A/B)}(\omega) = \frac{1}{3}\left(\frac{2}{\omega} + \frac{1}{\omega \mp U}\right) \text{ for } U = 2\Delta,\ T = 0. \quad (27)$$

The divergence of the above sublattice self-energies at $\omega = 0$ makes $\mathcal{F}_1$ divergent at this point and therefore gives rise to vanishing DOS and hence a Dirac point. Note that the existence of an intermediate Dirac phase which has been brought up with state-of-the-art DMFT now can be seen analytically using even a lowest-order expression for the auxiliary fermion self-energies. Therefore, the conducting phase that results from the competition between U and Δ does not seem to be an artifact of infinite dimensions inherent in DMFT formulation. Let us now go beyond the zeroth order and see how the spectral gap evolves upon going to higher orders of expansion.

TABLE I. The single-particle gap for the zeroth-order diagram of Fig. 1 at $\Delta = 4t$ and zero temperature.

U/t	2	8	12
E_{gap}/t	5.9558	0.0000	3.9998

B. Beyond zeroth order

Up to now, we have only considered the lowest-order diagram of Fig. 1. Let us now add the second-order diagram of Fig. 1. The self-energy of auxiliary fermions of second-order diagram on sublattice A ($\Gamma_2^{(A)}$) for arbitrary temperature is given in Appendix B 1. The one for sublattice B is obtained by simply changing the sign of Δ, i.e., $\Delta \to -\Delta$. We have used subscript 2 in $\Gamma_2^{(A)}$ to stress that this self-energy is only related to second-order diagram of Fig. 1. Note that self-energy of auxiliary fermions on sublattice A in expansion up to second order is obtained by adding Eq. (B2) to (25). Also, the zero-temperature limit of auxiliary fermion self-energies on two sublattices for second-order diagram is presented in Appendix B 1. Having $\Gamma^{(A)}$ and $\Gamma^{(B)}$, we are able to calculate the single-particle gap. The competition between interaction U and ionic potential Δ at $\Delta = 4t$ for zero temperature is shown in Fig. 7. This figure shows the value of gap as a

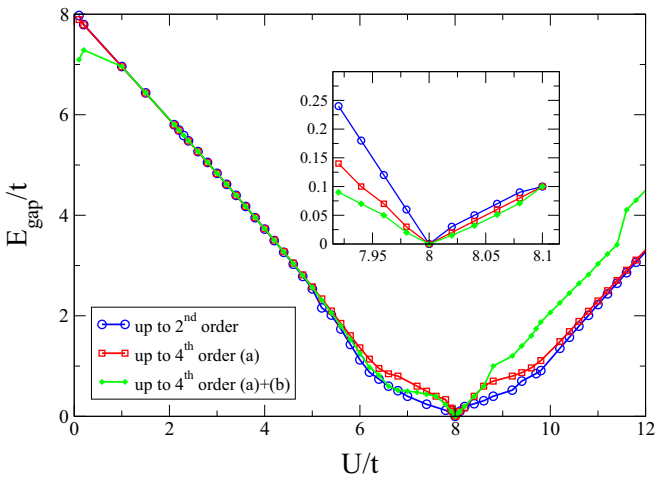

FIG. 7. Calculated single-particle gap of the half-filled ionic Hubbard model on honeycomb lattice in zero-temperature limit for $\Delta = 4t$ up to second order (blue circles), to fourth-order diagram 8(a) (red squares), and to both fourth-order diagrams of Fig. 8 (green diamonds). The inset zooms in the region around $U = 2\Delta$.

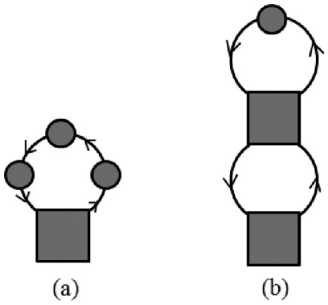

FIG. 8. Fourth-order diagrams contributed to self-energy of auxiliary fermions where squares and circles refer to two- and one-particle connected correlation functions, respectively. Solid lines also represent free propagator of auxiliary fermions.

function of U for a fixed $\Delta = 4t$ at zero temperature. The quantum critical metallic state is at $U = 8t$ that corresponds to $U = 2\Delta$ where the gap entirely vanishes, and the spectrum of excitation contains a Dirac cone. As pointed out earlier, the present strong-coupling scheme being an expansion in powers of t works better when the parameters satisfy $U, \Delta \gg t$. That is why we have chosen $\Delta = 4t$ to address the competition between U and Δ in presence of the hopping term.

As can be seen in Fig. 7 (blue circles), in the presence of Δ for two diagrams of Fig. 1, when the Hubbard interaction term U is small, there is a gap in the spectrum of single-particle excitation. Since this gap is continuously connected to the $U \to 0$ limit, this gapped phase is a band insulating state. When U increases, there is a critical point where the gap is zero, and the DOS is characterized by a Dirac cone around the $\omega = 0$. As U increases more, the system enters the Mott insulating phase. It is important to see that for small values of U/t, although the parameters fall outside of the expected region of convergence of the present strong-coupling approximation, the corresponding phases captured here are in qualitative agreement with our earlier studies using DMFT [32].

In order to better treat the quantum fluctuations on top of the classical Hamiltonian H_0 of the ionic Hubbard model (i.e., Δ and U terms involving commuting $n_{i\sigma}$ variables only), we consider higher orders in the perturbation theory. All fourth-order diagrams are demonstrated in Fig. 18 of Ref. [26], but to illustrate their effect on the gap magnitude near the critical Dirac state $U = 2\Delta$, we only consider two fourth-order diagrams that are depicted in Fig. 8. Since for other fourth-order diagrams, one needs to calculate three-particle connected correlation function which involves different expressions for 5! possible time orderings (one of the times can be set to zero) which makes it a formidable task to consider all of them. The self-energies of auxiliary fermions on sublattices A/B in the zero-temperature limit for fourth-order diagrams of Figs. 8(a) ($\Gamma^{(A/B)}_{4(a)}$) and 8(b) ($\Gamma^{(A/B)}_{4(b)}$) are given in Appendix B 2. The single-particle gaps obtained from adding diagram 8(a) (red squares) and both diagrams of Fig. 8 (green diamonds) to diagrams of Fig. 1 are shown in Fig. 7. As we see, by increasing the order of perturbation theory, the gap magnitudes for values of U around $U = 2\Delta$ become smaller (see inset of Fig. 7). However, the present partial fourth-order calculation is not enough to imply that the quantum critical point at $U = 2\Delta$ is broadened into a conducting (Dirac) region.

V. DISCUSSIONS AND SUMMARY

We have implemented a strong-coupling expansion based on formalism proposed by Pairault *et al.* in Ref. [25] on honeycomb lattice. We have used this method to study the semimetal to Mott insulator transition on honeycomb lattice systems such as graphene and silicene. We have also used the ionic Hubbard model to study the competition between the ionic potential (mass term) and the Hubbard U.

To study the influence of the onsite Coulomb interaction on honeycomb lattice, we have carried out the perturbative expansion of the auxiliary fermions around the atomic limit up to order $(t/U)^2$ and have analytically calculated the single-particle gap of the half-filled Hubbard model as function of U. The behavior of a closed-form function $\mathcal{F}(\omega)$ particularly at $\omega = 0$ contains a great deal of dynamical information about the possible interaction-induced gaps as well as about the Dirac nature of charge carriers on the honeycomb lattice. With this approach we find that the Mott transition for the Hubbard model on the honeycomb lattice occurs at $2.38t$. Although within the other various methods cited in Sec. I, it seems that the critical value for Mott transition is above 3, but since the present method is based on the strong-coupling expansion, it is natural for this method to emphasize the Mottness, unless one is able to perform the perturbation up to infinite order, which is not feasible.

In the second part of this paper we have studied the half-filled ionic Hubbard model on honeycomb lattice by strong-coupling perturbation theory up to fourth order in terms of the hopping amplitude t. We have found the limits $U < 2\Delta$ and $U > 2\Delta$ are gapped states corresponding to band and Mott insulating phases, respectively. In the interaction strength $U = 2\Delta$, owing to interplay between ionic potential and interaction, a semimetallic phase is restored. This agrees with earlier studies [31,32]. It is interesting that the present result has been extracted within lowest-, second-, and fourth-order diagrams in terms of the behavior of function $\mathcal{F}_1$, particularly around $\omega = 0$. The detailed functional form of this function depends on the particular order of the auxiliary fermion perturbation theory.

This study can be directly relevant to recent graphene/SiC where a gap of 0.5 eV has been found [3]. In this case, the gap of 0.5 eV is jointly determined by a single-particle gap parameter Δ and the many-particle (Mott) gap parameter U.

The present strong-coupling scheme seems to give reasonable results about the nature of the gap in the spectrum of excitation. The method seems to be capable of an unbiased estimate of the excitation spectrum in strongly correlated systems.

ACKNOWLEDGMENTS

E.A. was supported by the National Elite Foundation of Iran. S.A.J. was supported by the Alexander von Humboldt foundation, Germany.

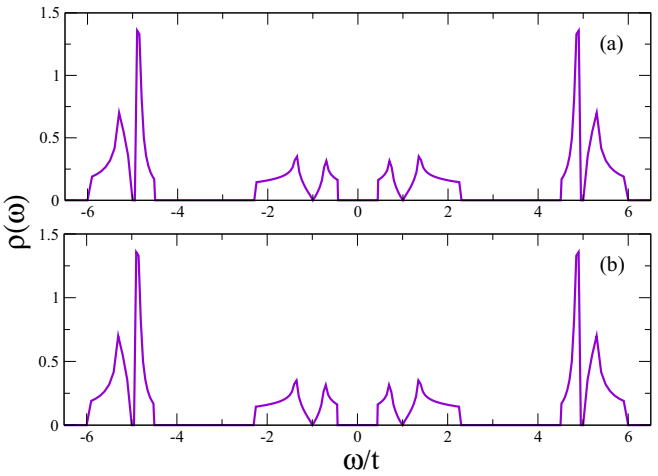

FIG. 9. DOS of the half-filled ionic Hubbard model on honeycomb lattice for $U = 6$, $\Delta = 2$, and $T = 0$ up to order t^2 obtained from (a) Eq. (A1) for $\eta = 10^{-4}$ and (b) Eq. (A6).

APPENDIX A: EXACT EXPRESSION FOR DOS ON HONEYCOMB LATTICE

We are going to represent the DOS of arbitrary complex frequency ξ on honeycomb lattice. According to Ref. [40], the DOS for tight-binding model on the honeycomb lattice can be expressed as

$$\rho = -\frac{1}{\pi}\sum_{\mathbf{k}} \mathrm{Im\ Tr}\, G(\xi,\mathbf{k}) = -\frac{1}{\pi}\,\mathrm{Im}\left[2\,\xi\; G_\xi\left(\frac{1}{2}(\xi^2-3);0,0\right)\right], \tag{A1}$$

where

$$G_\xi(\xi;0,0) = \frac{1}{2\pi}\; g\; \tilde{K}(k) \tag{A2}$$

is the local Green's function evaluated at general complex argument ξ, and g, k, and $\tilde{K}(k)$ are given as follows:

$$g = \frac{2}{[(2\xi+3)^{1/2}-1]^{3/2}[(2\xi+3)^{1/2}-1]^{1/2}}, \tag{A3}$$

$$k = \frac{4(2\xi+3)^{1/4}}{[(2\xi+3)^{1/2}-1]^{3/2}[(2\xi+3)^{1/2}-1]^{1/2}}, \tag{A4}$$

$$\tilde{K}(k) = \begin{cases} K(k), & \mathrm{Im}\xi > 0 \text{ and } \mathrm{Im}k < 0 \\ & \text{or } \mathrm{Im}\xi < 0 \text{ and } \mathrm{Im}k > 0, \\ K(k) + 2iK'(k), & \mathrm{Im}\xi > 0 \text{ and } \mathrm{Im}k > 0, \\ K(k) - 2iK'(k), & \mathrm{Im}\xi < 0 \text{ and } \mathrm{Im}k < 0, \end{cases} \tag{A5}$$

where $K(k)$ and $K'(k)$ are the complete elliptic integral of the first kind and the complete elliptic integral of the first kind with complementary modulus of k, respectively.

The above formula is quite general. However, in the $\eta \to 0$ limit it turns out that when $\xi = \mathrm{F}(\omega + i\eta)$, DOS (A1) reduces to

$$\rho(\omega) = \frac{|\mathrm{F}(\omega)|}{\pi^2}\frac{1}{\sqrt{Z_0}}\,K\left(\sqrt{\frac{Z_1}{Z_0}}\right), \tag{A6}$$

where Z_0 and Z_1 are those introduced in Eqs. (14) and (15), albeit substitute ω with $\mathrm{F}(\omega)$. If we assume ξ in Eq. (A1) has infinitesimal imaginary part, $\omega + i0^+$, the resulting DOS will be DOS of graphene. Also, DOS for the ionic Hubbard model on honeycomb lattice for $U = 6$, $\Delta = 2$, and $T = 0$ obtained from Eqs. (A1) and (A6) are shown on Figs. 9(a) and 9(b), respectively. As we can see, the two DOS well coincide, demonstrating that the above representation works well for situations where F is purely imaginary or purely real.

APPENDIX B: DUAL FERMION SELF-ENERGIES IN IONIC HUBBARD MODEL

This appendix gives the calculated self-energies of auxiliary fermions in second and fourth order.

1. Second order

Introducing the definitions

$$Z^{(A)} = 1 + 2e^{\beta(u-\Delta)} + e^{-2\beta\Delta}, \quad n_F(x) = \frac{1}{e^{\beta x}+1}, \quad n_B(x) = \frac{1}{e^{\beta x}-1}, \tag{B1}$$

the self-energy of the second-order diagram of Fig. 1 on sublattice A ($\Gamma_2^{(A)}$) at arbitrary temperature $1/\beta$ reads as

$$\begin{aligned}\Gamma_2^{(A)}(i\omega) = {} & \frac{-1.15\,t^2\,(2n^{(A)}-1)\,n_F(\Delta+u)}{(i\omega-\Delta)^2-u^2}\left(\frac{1-n^{(B)}}{\Delta+u}+\frac{n^{(B)}}{\Delta}\right) \\ & + \frac{2.3\,t^2\,(2n^{(A)}-1)\,n_B(2\Delta)}{(i\omega-\Delta)^2-u^2}\left(\frac{1-n^{(B)}}{i\omega-3\Delta-u}+\frac{n^{(B)}}{i\omega-3\Delta+u}\right) \\ & - \frac{1.15\,t^2}{(i\omega-\Delta)^2-u^2}\left(\beta u^2 n^{(A)}(1-n^{(A)}) + \frac{\beta u^2}{(Z^{(A)})^2}(e^{-2\beta\Delta}-e^{2\beta(u-\Delta)}) + u(1-n^{(A)})\right) \\ & \times\left\{(1-n^{(B)})\left(\frac{n_F(\Delta+u)}{u(\Delta+u)}+\frac{n_F(-\Delta-u)}{\Delta(\Delta+u)}-\frac{n_F(\Delta-u)}{\Delta u}\right) + n^{(B)}\left(\frac{n_F(\Delta+u)}{\Delta u}-\frac{n_F(\Delta-u)}{u(\Delta-u)}-\frac{n_F(-\Delta+u)}{\Delta(-\Delta+u)}\right)\right\}\end{aligned}$$

$$
\begin{aligned}
&+\frac{2.3\,t^2\,u\,(1-n^{(A)})}{(i\omega-\Delta)^2-u^2}\left\{(1-n^{(B)})\left(\frac{n_F(-\Delta-u)-n_F(\Delta-u)}{4\Delta^2}+\frac{-\beta\,n_F(\Delta-u)+\beta\,[n_F(\Delta-u)]^2}{2\Delta}\right)\right.\\
&\left.+n^{(B)}\left(\frac{n_F(-\Delta+u)-n_F(\Delta-u)}{4(\Delta-u)^2}+\frac{-\beta\,n_F(\Delta-u)+\beta\,[n_F(\Delta-u)]^2}{2(\Delta-u)}\right)\right\}\\
&+\frac{1.15\,t^2\,((i\omega-\Delta)(2n^{(A)}-1)+u)}{(i\omega-\Delta)^2-u^2}\left\{(1-n^{(B)})\right.\\
&\times\left(\frac{n_F(-\Delta-u)-n_F(\Delta+u)}{4(\Delta+u)^2}+\frac{-\beta\,n_F(\Delta+u)+\beta\,[n_F(\Delta+u)]^2}{2(\Delta+u)}\right)\\
&\left.+n^{(B)}\left(\frac{n_F(-\Delta+u)-n_F(\Delta+u)}{4\Delta^2}+\frac{-\beta\,n_F(\Delta+u)+\beta\,[n_F(\Delta+u)]^2}{2\Delta}\right)\right\}\\
&+\frac{4.6\,t^2\,u^2}{[(i\omega-\Delta)^2-u^2]^2}\left(\frac{1-n^{(B)}}{i\omega+\Delta+u}+\frac{n^{(B)}}{i\omega+\Delta-u}\right)\left(n^{(A)}(1-n^{(A)})+\frac{e^{\beta(u-\Delta)}}{Z^{(A)}}\right)\\
&+1.15\,t^2\,u\left(\frac{(1-n^{(A)})}{2\,(i\omega-\Delta+u)^2}+\frac{1}{4\,(i\omega-\Delta-u)^2}\right)\\
&\times\left\{(1-n^{(B)})\left(\frac{n_F(\Delta+u)}{u(\Delta+u)}+\frac{n_F(-\Delta-u)}{\Delta(\Delta+u)}-\frac{n_F(\Delta-u)}{\Delta u}\right)+n^{(B)}\left(\frac{n_F(\Delta+u)}{\Delta u}-\frac{n_F(\Delta-u)}{u(\Delta-u)}-\frac{n_F(-\Delta+u)}{\Delta(-\Delta+u)}\right)\right\}\\
&+\frac{1.15\,t^2\,(2n^{(A)}-1)}{4\,(i\omega-\Delta-u)^2}\left\{(1-n^{(B)})\left(\frac{n_F(\Delta-u)}{\Delta}+\frac{n_F(\Delta+u)}{\Delta+u}-\frac{(2\Delta+u)\,n_F(-\Delta-u)}{\Delta(\Delta+u)}\right)\right.\\
&\left.+n^{(B)}\left(\frac{n_F(\Delta-u)}{\Delta-u}+\frac{n_F(\Delta+u)}{\Delta}+\frac{(2\Delta-u)\,n_F(-\Delta+u)}{\Delta(-\Delta+u)}\right)\right\}\\
&-\frac{1.15\,t^2\,(2n^{(A)}-1)}{(i\omega-\Delta-u)^2}\left\{\frac{(1-n^{(B)})(n_F(-\Delta-u)+n_B(2\Delta))}{i\omega-3\Delta-u}+\frac{n^{(B)}(n_F(-\Delta+u)+n_B(2\Delta))}{i\omega-3\Delta+u}\right\}\\
&-\frac{1.15\,t^2\,(2n^{(A)}-1)}{(i\omega-\Delta+u)^2}\left\{n_B(2\Delta)\left(\frac{1-n^{(B)}}{i\omega-3\Delta-u}+\frac{n^{(B)}}{i\omega-3\Delta+u}\right)\right.\\
&\left.-n_F(\Delta+u)\left(\frac{n^{(B)}(i\omega+\Delta+u)}{4\Delta^2}+\frac{(1-n^{(B)})(i\omega+\Delta+3u)}{4(\Delta+u)^2}\right)\right\}\\
&+\frac{1.15\,t^2\,(2n^{(A)}-1)}{2\,(i\omega-\Delta+u)}(\beta\,n_F(\Delta+u)-\beta\,[n_F(\Delta+u)]^2)\left(\frac{1-n^{(B)}}{\Delta+u}+\frac{n^{(B)}}{\Delta}\right)\\
&-\frac{1.15\,t^2\,(2n^{(A)}-1)\,n^{(B)}\,n_F(-\Delta+u)}{i\omega-3\Delta+u}\left(\frac{1}{4\Delta^2}-\frac{1}{\Delta\,(i\omega-\Delta-u)}\right)\\
&-\frac{1.15\,t^2\,(2n^{(A)}-1)\,(1-n^{(B)})\,n_F(-\Delta-u)}{i\omega-3\Delta-u}\left(\frac{1}{4(\Delta+u)^2}-\frac{1}{(\Delta+u)\,(i\omega-\Delta-u)}\right),
\end{aligned}
\tag{B2}
$$

where $u=U/2$ and $n^{(A)}$, $n^{(B)}$ are given in Eq. (24). By flipping the sign of Δ in the self-energy $\Gamma_2^{(A)}$ of sublattice A, one can obtain the self-energy of auxiliary fermions on sublattice B in given order ($\Gamma_2^{(B)}$). Taking the zero-temperature limit, the second-order self-energy of auxiliary fermions on sublattices A and B is simplified to

$$
\Gamma_2^{(A)}(i\tilde{\omega})=\begin{cases}
\frac{1.15\tilde{t}^2}{\Delta}\left[\frac{-\tilde{u}^2}{2(\tilde{u}^2-1)^2[(i\tilde{\omega}-1)^2-\tilde{u}^2]}+\frac{3\tilde{u}^2(i\tilde{\omega}+1)}{[(i\tilde{\omega}-1)^2-\tilde{u}^2]^2[(i\tilde{\omega}+1)^2-\tilde{u}^2]}+\frac{1}{4(\tilde{u}^2-1)}\left(\frac{1}{(i\tilde{\omega}+\tilde{u}-1)}+\frac{1}{(i\tilde{\omega}-\tilde{u}-1)}\right)^2\right], & \tilde{u}>1\\
\infty, & \tilde{u}=1\\
\frac{1.15\tilde{t}^2}{\Delta}\left[\frac{\tilde{u}}{[(i\tilde{\omega}-1)^2-\tilde{u}^2]}\left(\frac{1}{2(1-\tilde{u})^2}-\frac{1}{(1-\tilde{u})}\right)-\frac{1}{4(i\tilde{\omega}+\tilde{u}-1)}+\frac{1}{2(1-\tilde{u})}\left(\frac{1}{(i\tilde{\omega}-\tilde{u}-1)^2}+\frac{\tilde{u}}{(i\tilde{\omega}+\tilde{u}-1)^2}\right)\right.\\
\quad\left.+\frac{1}{(i\tilde{\omega}+\tilde{u}-3)}\left(\frac{1}{(i\tilde{\omega}-\tilde{u}-1)}-\frac{1}{2}\right)^2\right], & \tilde{u}<1
\end{cases}
\tag{B3}
$$

and

$$\Gamma_2^{(B)}(i\tilde{\omega}) = \begin{cases} \frac{1.15\tilde{t}^2}{\Delta}\Big[\frac{\tilde{u}^2}{2(\tilde{u}^2-1)^2[(i\tilde{\omega}+1)^2-\tilde{u}^2]} + \frac{3\tilde{u}^2(i\tilde{\omega}-1)}{[(i\tilde{\omega}+1)^2-\tilde{u}^2]^2[(i\tilde{\omega}-1)^2-\tilde{u}^2]} - \frac{1}{4(\tilde{u}^2-1)}\Big(\frac{1}{(i\tilde{\omega}+\tilde{u}+1)} + \frac{1}{(i\tilde{\omega}-\tilde{u}+1)}\Big)^2\Big], & \tilde{u} > 1 \\ \infty, & \tilde{u} = 1 \\ \frac{1.15\tilde{t}^2}{\Delta}\Big[\frac{-1}{(\tilde{u}-1)[(i\tilde{\omega}+1)^2-\tilde{u}^2]} - \frac{1}{4(\tilde{u}-1)^2(i\tilde{\omega}-\tilde{u}+1)} + \frac{1}{2(\tilde{u}-1)[i\tilde{\omega}-\tilde{u}+1]^2} + \frac{(i\tilde{\omega}+3\tilde{u}-1)}{4(\tilde{u}+1)^2(i\tilde{\omega}+\tilde{u}+1)^2} \\ \quad + \frac{1}{(i\tilde{\omega}-\tilde{u}+3)}\Big(\frac{1}{(i\tilde{\omega}-\tilde{u}+1)} - \frac{1}{(i\tilde{\omega}+\tilde{u}+1)}\Big)^2\Big], & \tilde{u} < 1 \end{cases} \tag{B4}$$

where we have used dimensionless quantities $\tilde{t} = \frac{t}{\Delta}$, $\tilde{\omega} = \frac{\omega}{\Delta}$, and $\tilde{u} = \frac{u}{\Delta}$. It is interesting to note that the above expressions have an overall scale $\tilde{t}^2/\Delta$ multiplied by a function of ω/Δ and u/Δ. This scaling functional form continues to higher order as we see in the next subsection.

2. Fourth order

We have undertaken the cumbersome task of calculation of two of the fourth-order diagrams discussed in the text. The arbitrary temperature expression for the fourth-order contributions is huge. Therefore, in this appendix we only report their zero-temperature limit. The zero-temperature limit of self-energies of auxiliary fermions on sublattices A/B corresponding to diagrams 8(a) ($\Gamma^{(A/B)}_{4(a)}$) and 8(b) ($\Gamma^{(A/B)}_{4(b)}$) are separately calculated in two regions $u > \Delta(\tilde{u} > 1)$ and $u < \Delta(\tilde{u} < 1)$. This separation naturally arises when we take the zero-temperature limit.

In the $\tilde{u} > 1$ limit, the self-energies are given by

$$\begin{aligned}\Gamma^{(A)}_{4(a)}(i\tilde{\omega}) = \frac{\tilde{t}^4}{\Delta}\Bigg[&\frac{3\tilde{u}^2}{8[(i\tilde{\omega}-1)^2-\tilde{u}^2]^2}\Big(\frac{1}{i\tilde{\omega}+\tilde{u}+1}+\frac{1}{i\tilde{\omega}-\tilde{u}+1}\Big)^2\Big(\frac{1}{i\tilde{\omega}+\tilde{u}-1}+\frac{1}{i\tilde{\omega}-\tilde{u}-1}\Big)\\ &+\frac{\tilde{u}}{8}\Big(\frac{1}{(i\tilde{\omega}+\tilde{u}-1)^2}+\frac{1}{(i\tilde{\omega}-\tilde{u}-1)^2}\Big)\Big(\frac{(\tilde{u}+1)^2+1}{8\tilde{u}(\tilde{u}+1)^3}-\frac{\tilde{u}+2}{8(\tilde{u}+1)^2}+\frac{1}{8\tilde{u}^2(1-\tilde{u})^3}+\frac{\tilde{u}-1}{8\tilde{u}^2}\Big)+\frac{\tilde{u}}{8[(i\tilde{\omega}-1)^2-\tilde{u}^2]}\\ &\times\Big(-\frac{\tilde{u}+2}{8\tilde{u}(\tilde{u}+1)^2}+\frac{\tilde{u}-2}{8\tilde{u}(\tilde{u}-1)^2}+\frac{5\tilde{u}-2}{16\tilde{u}(\tilde{u}-1)^4}+\frac{2\tilde{u}^2+7\tilde{u}+3}{16(\tilde{u}+1)^3}+\frac{2-\tilde{u}}{16\tilde{u}(\tilde{u}+1)^4}+\frac{2\tilde{u}^2-3\tilde{u}+7}{16(1-\tilde{u})^3}\Big)\Bigg],\end{aligned} \tag{B5}$$

$$\begin{aligned}\Gamma^{(B)}_{4(a)}(i\tilde{\omega}) = \frac{\tilde{t}^4}{\Delta}\Bigg[&\frac{3\tilde{u}^2}{8[(i\tilde{\omega}+1)^2-\tilde{u}]^2}\Big(\frac{1}{i\tilde{\omega}+\tilde{u}-1}+\frac{1}{i\tilde{\omega}-\tilde{u}-1}\Big)^2\Big(\frac{1}{i\tilde{\omega}+\tilde{u}+1}+\frac{1}{i\tilde{\omega}-\tilde{u}+1}\Big)\\ &+\frac{\tilde{u}}{8}\Big(\frac{1}{(i\tilde{\omega}+\tilde{u}+1)^2}+\frac{1}{(i\tilde{\omega}-\tilde{u}+1)^2}\Big)\Big(\frac{(\tilde{u}-1)^2+1}{8\tilde{u}(\tilde{u}-1)^3}+\frac{\tilde{u}-2}{8(\tilde{u}-1)^2}+\frac{1}{8\tilde{u}^2(\tilde{u}+1)^3}-\frac{\tilde{u}+1}{8\tilde{u}^2}\Big)\\ &+\frac{\tilde{u}}{8[(i\tilde{\omega}+1)^2-\tilde{u}^2]}\Big(\frac{2-\tilde{u}}{8\tilde{u}(\tilde{u}-1)^2}+\frac{\tilde{u}+2}{8\tilde{u}(\tilde{u}+1)^2}+\frac{5\tilde{u}+2}{16\tilde{u}(\tilde{u}+1)^4}-\frac{2\tilde{u}^2-7\tilde{u}+3}{16(\tilde{u}-1)^3}-\frac{\tilde{u}+2}{16\tilde{u}(\tilde{u}-1)^4}+\frac{2\tilde{u}^2+3\tilde{u}+7}{16(\tilde{u}+1)^3}\Big)\Bigg],\end{aligned} \tag{B6}$$

$$\begin{aligned}\Gamma^{(A)}_{4(b)}(i\tilde{\omega}) = \frac{(1.15)^2\tilde{t}^4}{\Delta}\Bigg[&-\frac{9\,\tilde{u}^4}{4[(i\tilde{\omega}-1)^2-\tilde{u}^2]^2\,[(i\tilde{\omega}+1)^2-\tilde{u}^2]^2}\Big(\frac{1}{i\tilde{\omega}+\tilde{u}-1}+\frac{1}{i\tilde{\omega}-\tilde{u}-1}\Big)\\ &+\frac{\tilde{u}^2}{8(\tilde{u}^2-1)\,[(i\tilde{\omega}-1)^2-\tilde{u}^2]^2}\Big(\frac{1}{i\tilde{\omega}+\tilde{u}+1}-\frac{1}{i\tilde{\omega}-\tilde{u}+1}\Big)^2-\frac{\tilde{u}^4}{4\,(\tilde{u}^2-1)^2\,[(i\tilde{\omega}-1)^2-\tilde{u}^2]^2\,[(i\tilde{\omega}+1)^2-\tilde{u}^2]}\\ &-\frac{(4\tilde{u}^3-3\tilde{u}^2-2\tilde{u}+1)}{64\,(\tilde{u}^2-1)^2\,(\tilde{u}-1)^2}\Big(\frac{1}{i\tilde{\omega}+\tilde{u}-1}-\frac{1}{i\tilde{\omega}-\tilde{u}-1}\Big)^2\\ &+\frac{3}{128}\Big(\frac{\tilde{u}^3+4\tilde{u}^2+6\tilde{u}+2}{(1+\tilde{u})^3}-\frac{\tilde{u}^2(\tilde{u}-2)}{(\tilde{u}-1)^3}\Big)\Big(\frac{1}{(i\tilde{\omega}+\tilde{u}-1)^2}+\frac{1}{(i\tilde{\omega}-\tilde{u}-1)^2}\Big)\\ &+\frac{1}{2[(i\tilde{\omega}-1)^2-\tilde{u}^2]}\Big(\frac{3(3\tilde{u}+2)}{128}-\frac{3\tilde{u}^3(3\tilde{u}^2+4)}{128(\tilde{u}-1)^4}+\frac{(1+\tilde{u}^2)(\tilde{u}^4+2\tilde{u}^2-1)}{16(\tilde{u}^2-1)^4}+\frac{3\tilde{u}^2}{32(\tilde{u}-1)^2}\\ &-\frac{3(\tilde{u}^4+5\tilde{u}^3+10\tilde{u}^2+3\tilde{u})}{64(\tilde{u}+1)^4}\Big)\Bigg],\end{aligned} \tag{B7}$$

$$\Gamma^{(B)}_{4(b)}(i\tilde{\omega}) = \frac{(1.15)^2\tilde{t}^4}{\Delta}\Bigg[\frac{-9\tilde{u}^4}{4[(i\tilde{\omega}+1)^2-\tilde{u}^2]^2[(i\tilde{\omega}-1)^2-\tilde{u}^2]^2}\left(\frac{1}{i\tilde{\omega}+\tilde{u}+1}+\frac{1}{i\tilde{\omega}-\tilde{u}+1}\right)$$
$$+\frac{\tilde{u}^2}{8(1-\tilde{u}^2)[(i\tilde{\omega}+1)^2-\tilde{u}^2]^2}\left(\frac{1}{i\tilde{\omega}+\tilde{u}-1}-\frac{1}{i\tilde{\omega}-\tilde{u}-1}\right)^2$$
$$+\frac{\tilde{u}^4}{4(\tilde{u}^2-1)^2[(i\tilde{\omega}^2+1)^2-\tilde{u}^2]^2[(i\tilde{\omega}-1)^2-\tilde{u}^2]}-\frac{(4\tilde{u}^3+3\tilde{u}^2-2\tilde{u}-1)}{64(1+\tilde{u})^2(\tilde{u}^2-1)^2}\left(\frac{1}{i\tilde{\omega}+\tilde{\omega}+1}-\frac{1}{i\tilde{\omega}-\tilde{u}+1}\right)^2$$
$$+\frac{3}{128}\left(\frac{\tilde{u}^2(\tilde{u}+2)}{(\tilde{u}+1)^3}-\frac{\tilde{u}^3-4\tilde{u}^2+6\tilde{u}-2}{(\tilde{u}-1)^3}\right)\left(\frac{1}{(i\tilde{\omega}-\tilde{u}+1)^2}+\frac{1}{(i\tilde{\omega}+\tilde{u}+1)^2}\right)$$
$$-\frac{1}{2[(i\omega+1)^2-\tilde{u}^2]}\left(\frac{-3(3\tilde{u}-2)}{128}+\frac{3\tilde{u}^3(3\tilde{u}^2+4)}{128(\tilde{u}+1)^4}+\frac{(\tilde{u}^2+1)(\tilde{u}^4+2\tilde{u}^2+1)}{16(\tilde{u}^2-1)^4}+\frac{3\tilde{u}^2}{32(\tilde{u}+1)^2}\right.$$
$$\left.-\frac{3(\tilde{u}^4-5\tilde{u}^3+10\tilde{u}^2-3\tilde{u})}{64(\tilde{u}-1)^4}\right)\Bigg]. \tag{B8}$$

In the $\tilde{u}<1$, the self-energies are expressed as

$$\Gamma^{(A)}_{4(a)}(i\tilde{\omega}) = \frac{-\tilde{t}^4}{\Delta}\Bigg[\frac{1}{(i\tilde{\omega}-\tilde{u}-1)^2}\left(\frac{1}{2(\tilde{u}-1)(i\tilde{\omega}+\tilde{u}-3)^2}+\frac{1}{4(\tilde{u}-1)^2(i\tilde{\omega}+\tilde{u}-3)}+\frac{1}{16(\tilde{u}-1)}+\frac{(\tilde{u}-3)(\tilde{u}+1)}{16(\tilde{u}-1)^3}\right)$$
$$-\frac{2}{(i\tilde{\omega}-\tilde{u}-1)(i\tilde{\omega}+\tilde{u}-3)}\left(\frac{1}{4(\tilde{u}-1)(i\tilde{\omega}+\tilde{u}-3)}-\frac{\tilde{u}-2}{8(\tilde{u}-1)^2}\right)+\frac{\tilde{u}}{[(i\tilde{\omega}-1)^2-\tilde{u}^2]}\left(\frac{3}{8(\tilde{u}-1)^4}+\frac{4(3-\tilde{u})}{16(\tilde{u}-1)^3}\right)$$
$$+\frac{2\tilde{u}(\tilde{u}-3)}{16(\tilde{u}-1)^3(i\tilde{\omega}+\tilde{u}-1)^2}+\frac{2\tilde{u}-3}{16(\tilde{u}-1)^2(i\tilde{\omega}+\tilde{u}-1)}+\frac{3-2\tilde{u}}{16(\tilde{u}-1)^2(i\tilde{\omega}+\tilde{u}-3)}+\frac{1}{8(\tilde{u}-1)(i\tilde{\omega}+\tilde{u}-3)^2}\Bigg], \tag{B9}$$

$$\Gamma^{(B)}_{4(a)} = \frac{-\tilde{t}^4}{\Delta}\Bigg[\frac{1}{(i\tilde{\omega}+\tilde{u}+1)}\left(\frac{-1}{(i\tilde{\omega}-\tilde{u}+1)^2(i\tilde{\omega}-\tilde{u}+3)^2}+\frac{1}{4(\tilde{u}-1)^2(i\tilde{\omega}-\tilde{u}+1)^2}-\frac{1}{(i\tilde{\omega}+\tilde{u}+1)^2(i\tilde{\omega}-\tilde{u}+3)^2}\right.$$
$$\left.+\frac{1}{4(\tilde{u}-1)^2(i\tilde{\omega}+\tilde{u}+1)^2}+\frac{3}{16(\tilde{u}-1)^4}\right)$$
$$+\frac{1}{i\tilde{\omega}-\tilde{u}+1}\left(\frac{2}{(i\tilde{\omega}+\tilde{u}+1)^2(i\tilde{\omega}-\tilde{u}+3)^2}-\frac{1}{2(\tilde{u}-1)^2(i\tilde{\omega}+\tilde{u}+1)^2}-\frac{1}{2(\tilde{u}-1)^3(i\tilde{\omega}+\tilde{u}+1)}-\frac{3}{16(\tilde{u}-1)^4}\right)$$
$$+\frac{1}{8(\tilde{u}-1)^2(i\tilde{\omega}-\tilde{u}+1)^2}\Bigg], \tag{B10}$$

$$\Gamma^{(A)}_{4(b)}(i\tilde{\omega}) = \frac{(1.15)^2\tilde{t}^4}{\Delta}\Bigg[\frac{1}{(i\tilde{\omega}-\tilde{u}-1)^2}\Bigg[\frac{1}{8(i\tilde{\omega}-\tilde{u}-5)}\left(1+\frac{1}{\tilde{u}-1}\right)^2+\frac{(1+\tilde{u})^2-3(\tilde{u}^2-1)}{16\tilde{u}(\tilde{u}-1)(i\tilde{\omega}+\tilde{u}-3)}-\frac{3\tilde{u}-2}{4\tilde{u}(\tilde{u}-1)^2(i\tilde{\omega}-\tilde{u}-3)}$$
$$-\frac{1}{4\tilde{u}(i\tilde{\omega}+\tilde{u}-1)}-\frac{1}{4(i\tilde{\omega}+\tilde{u}-3)^2}+\frac{1}{2(\tilde{u}-1)(i\tilde{\omega}-\tilde{u}-3)^2}\Bigg]$$
$$+\frac{1}{(i\tilde{\omega}-\tilde{u}-1)}\left(\frac{2\tilde{u}-1}{2\tilde{u}(\tilde{u}^2-1)^2(i\tilde{\omega}-\tilde{u}-3)}+\frac{\tilde{u}-2}{4\tilde{u}(\tilde{u}-1)(i\tilde{\omega}+\tilde{u}-3)}+\frac{2-\tilde{u}^2}{16(\tilde{u}-1)^2(i\tilde{\omega}+\tilde{u}-5)}\right.$$
$$\left.-\frac{1}{2(\tilde{u}^2-1)(i\tilde{\omega}-\tilde{u}-3)^2}+\frac{1}{8(i\tilde{\omega}+\tilde{u}-3)^2}\right)$$
$$+\frac{1}{128(i\tilde{\omega}+\tilde{u}-5)}\left(1+\frac{1}{\tilde{u}-1}\right)^2+\frac{\tilde{u}+(\tilde{u}-2)^2}{32\tilde{u}(\tilde{u}-1)(i\tilde{\omega}+\tilde{u}-3)}-\frac{(\tilde{u}-1)^2+\tilde{u}+1}{16\tilde{u}(1+\tilde{u})(\tilde{u}^2-1)^2(i\tilde{\omega}-\tilde{u}-3)}$$
$$-\frac{1}{16(i\tilde{\omega}+\tilde{u}-3)^2}\frac{1}{8(\tilde{u}-1)(1+\tilde{u})^2(i\tilde{\omega}-\tilde{u}-3)^2}$$
$$+\frac{\tilde{u}}{[(i\tilde{\omega}-1)^2-\tilde{u}^2]}\left(\frac{(\tilde{u}-1)^3+2\tilde{u}}{4\tilde{u}(\tilde{u}^2-1)^2}+\frac{\tilde{u}+(\tilde{u}-1)^2}{16(\tilde{u}-1)(\tilde{u}-2)^2}+\frac{1}{4\tilde{u}(1-\tilde{u})}+\frac{2\tilde{u}^2-3\tilde{u}+1}{16(\tilde{u}-1)^4}+\frac{1-4\tilde{u}}{16(\tilde{u}-1)^2}\right)$$
$$+\frac{1}{(i\tilde{\omega}+\tilde{u}-1)}\left(\frac{-9}{128}-\frac{1}{128(\tilde{u}-1)^2}+\frac{1}{8(\tilde{u}-1)(1+\tilde{u})^3}+\frac{3\tilde{u}-4}{128\tilde{u}(\tilde{u}-1)}-\frac{(\tilde{u}+1)^2+(\tilde{u}-1)(\tilde{u}+2)}{32(\tilde{u}^2-1)^2}\right)$$

$$+\frac{1}{32(i\omega-\tilde{u}-1)^2}\left(\frac{(\tilde{u}+1)(\tilde{u}-3)}{(\tilde{u}-1)^3}+\frac{5}{(2-\tilde{u})(\tilde{u}-1)}+\frac{2\tilde{u}-1}{\tilde{u}(2-\tilde{u})}+\frac{-2\tilde{u}^2+\tilde{u}-1}{\tilde{u}(\tilde{u}-1)^2}\right)$$
$$+\frac{\tilde{u}}{(i\omega+\tilde{u}-1)^2}\left(\frac{\tilde{u}+(\tilde{u}-1)^2}{32(\tilde{u}-1)^2(2-\tilde{u})}+\frac{-\tilde{u}^3-3\tilde{u}^2+\tilde{u}+1}{8\tilde{u}(\tilde{u}^2-1)^2}+\frac{\tilde{u}-2}{8(\tilde{u}-1)^3}\right)\Bigg], \tag{B11}$$

$$\Gamma^{(B)}_{4(b)}=\frac{(1.15)^2\tilde{t}^4}{\Delta}\Bigg[\frac{1}{2(i\tilde{\omega}-\tilde{u}+1)^2}\left(\frac{1}{(i\tilde{\omega}-\tilde{u}+5)(i\tilde{\omega}+\tilde{u}+3)^2}+\frac{1}{4(i\tilde{\omega}-\tilde{u}+5)}+\frac{1}{(i\tilde{\omega}+\tilde{u}+3)(i\tilde{\omega}-\tilde{u}+5)}\right.$$
$$\left.+\frac{(\tilde{u}-1)^3-2\tilde{u}^3}{4(\tilde{u}-1)^2[(i\tilde{\omega}+3)^2-\tilde{u}^2]}+\frac{1}{2(\tilde{u}-1)(i\tilde{\omega}+\tilde{u}+3)^2}-\frac{i\tilde{\omega}+2}{4[(i\tilde{\omega}+3)^2-\tilde{u}^2]}-\frac{1}{2(\tilde{u}-2)}+\frac{3}{8(\tilde{u}-1)^2}+\frac{1+\tilde{u}}{16\tilde{u}}\right)$$
$$+\frac{1}{(i\tilde{\omega}-\tilde{u}+1)}\left(\frac{-1}{(i\tilde{\omega}+\tilde{u}+1)(i\tilde{\omega}-\tilde{u}+5)(i\tilde{\omega}+\tilde{u}+3)^2}+\frac{1}{2(\tilde{u}-2)(i\tilde{\omega}+\tilde{u}+1)}-\frac{1}{4(i\tilde{\omega}+\tilde{u}+1)(i\tilde{\omega}-\tilde{u}+5)}\right.$$
$$-\frac{1}{(i\tilde{\omega}+\tilde{u}+1)(i\tilde{\omega}+\tilde{u}+3)(i\tilde{\omega}-\tilde{u}+5)}+\frac{\tilde{u}-3}{16(\tilde{u}-1)(i\tilde{\omega}+\tilde{u}+1)}-\frac{1}{2(\tilde{u}-1)(i\tilde{\omega}+\tilde{u}+1)(i\tilde{\omega}+\tilde{u}+3)^2}$$
$$+\frac{i\tilde{\omega}+2}{4(i\tilde{\omega}+\tilde{u}+1)[(i\tilde{\omega}+3)^2-\tilde{u}^2]}+\frac{2\tilde{u}^3+(1-\tilde{u})^3}{4(\tilde{u}-1)^2(i\tilde{\omega}+\tilde{u}+1)[(i\tilde{\omega}+3)^2-\tilde{u}^2]}-\frac{2\tilde{u}^3+(1-\tilde{u})^3}{16(\tilde{u}-1)^3(i\tilde{\omega}+\tilde{u}+1)}$$
$$\left.+\frac{\tilde{u}-3}{4(\tilde{u}-2)^2}+\frac{7\tilde{u}-5}{64(\tilde{u}-1)^2}-\frac{\tilde{u}(\tilde{u}+2)}{32(\tilde{u}-1)^4}\right)$$
$$+\frac{1}{2(i\tilde{\omega}+\tilde{u}+1)^2}\left(\frac{1}{(i\tilde{\omega}-\tilde{u}+5)(i\tilde{\omega}+\tilde{u}+3)}+\frac{1}{4(i\tilde{\omega}-\tilde{u}+5)}+\frac{2\tilde{u}^3-(\tilde{u}-1)^3}{4(\tilde{u}-1)^2[(i\tilde{\omega}+3)^2-\tilde{u}^2]}-\frac{1}{4(i\tilde{\omega}+\tilde{u}+3)^2}\right.$$
$$\left.\times\frac{1}{2(\tilde{u}-1)(i\tilde{\omega}+\tilde{u}+3)^2}-\frac{(i\tilde{\omega}+2)}{4[(i\tilde{\omega}+3)^2-\tilde{u}^2]}-\frac{1}{2(\tilde{u}-2)}+\frac{2-\tilde{u}}{8(\tilde{u}-1)}+\frac{\tilde{u}^3}{4(\tilde{u}-1)^3}\right)$$
$$+\frac{1}{(i\tilde{\omega}+\tilde{u}+1)}\left(\frac{\tilde{u}-3}{32(\tilde{u}-1)}+\frac{\tilde{u}-3}{8(\tilde{u}-2)^2}-\frac{\tilde{u}^3(\tilde{u}-2)}{32(\tilde{u}-1)^4}\right)\Bigg], \tag{B12}$$

where, as before, $\tilde{t}=\frac{t}{\Delta}$, $\tilde{\omega}=\frac{\omega}{\Delta}$, and $\tilde{u}=\frac{u}{\Delta}$.

[1] Y. Araki and T. Hatsuda, Chiral gap and collective excitations in monolayer graphene from strong coupling expansion of lattice gauge theory, Phys. Rev. B **82**, 121403 (2010).

[2] G. W. Semenoff, Chiral symmetry breaking in graphene, Phys. Scr. T **146**, 014016 (2012).

[3] M. S. Nevius, M. Conrad, F. Wang, A. Celis, M. N. Nair, A. Taleb-Ibrahimi, A. Tejeda, and E. H. Conrad, Semiconducting Graphene from Highly Ordered Substrate Interactions, Phys. Rev. Lett. **115**, 136802 (2015).

[4] T. O. Wehling, E. Şaşioğlu, C. Friedrich, A. I. Lichtenstein, M. I. Katsnelson, and S. Blügel, Strength of Effective Coulomb Interactions in Graphene and Graphite, Phys. Rev. Lett. **106**, 236805 (2011).

[5] M. Schuler, M. Rosner, T. O. Wehling, A. I. Lichtenstein, and M. I. Katsnelson, Optimal Hubbard Models for Materials with Nonlocal Coulomb Interactions: Graphene, Silicene, and Benzene, Phys. Rev. Lett. **111**, 036601 (2013).

[6] S. Sorella and E. Tosatti, Semi-metal-insulator transition of the Hubbard model in the honeycomb lattice, Europhys. Lett. **19**, 699 (1992).

[7] I. F. Herbut, Interactions and Phase Transitions on Graphenes Honeycomb Lattice, Phys. Rev. Lett. **97**, 146401 (2006).

[8] C. Honerkamp, Density Waves and Cooper Pairing on the Honeycomb Lattice, Phys. Rev. Lett. **100**, 146404 (2008).

[9] S. A. Jafari, Dynamical mean field study of the Dirac liquid, Eur. Phys. J. B **68**, 537 (2009).

[10] M. T. Tran and K. Kuroki, Finite-temperature semimetal-insulator transition on the honeycomb lattice, Phys. Rev. B **79**, 125125 (2009).

[11] R-Q. He and Z-Y. Lu, Cluster dynamical mean field theory of quantum phases on a honeycomb lattice, Phys. Rev. B **86**, 045105 (2012).

[12] W. Wu, Y.-H. Chen, H.-sh. Tao, N.-H. Tong, and W.-M. Liu, Interacting Dirac fermions on honeycomb lattice, Phys. Rev. B **82**, 245102 (2010).

[13] A. Liebsch, Correlated Dirac fermions on the honeycomb lattice studied within cluster dynamical mean field theory, Phys. Rev. B **83**, 035113 (2011).

[14] A. Vaezi and X.-G. Wen, Phase diagram of the Hubbard model on honeycomb lattice, arXiv:1010.5744v1.

[15] Z. Y. Meng, T. C. Lang, S. Wessel, F. F. Assaad, and A. Muramatsu, Quantum spin-liquid emerging in two-dimensional correlated Dirac fermions, Nature (London) **464**, 847 (2010).

[16] S.-L. Yu, X. C. Xie, and J.-X. Li, Mott Physics and Topological Phase Transition in Correlated Dirac Fermions, Phys. Rev. Lett. **107**, 010401 (2011).

[17] W. Wu, S. Rachel, W.-M. Liu, and K. Le Hur, Quantum spin Hall insulators with interactions and lattice anisotropy, Phys. Rev. B **85**, 205102 (2012).
[18] Q. Chen, G. H. Booth, S. Sharma, G. Knizia, and G. K.-L. Chan, Intermediate and spin-liquid phase of the half-filled honeycomb Hubbard model, Phys. Rev. B **89**, 165134 (2014).
[19] S. Sorella, Y. Otsuka, and S. Yunoki, Absence of a spin liquid phase in the Hubbard model on the honeycomb lattice, Sci. Rep. **2**, 992 (2012).
[20] S. R. Hassan and D. Sénéchal, Absence of Spin Liquid in Nonfrustrated Correlated Systems, Phys. Rev. Lett. **110**, 096402 (2013).
[21] F. F. Assaad and I. F. Herbut, Pinning the Order: The Nature of Quantum Criticality in the Hubbard Model on Honeycomb Lattice, Phys. Rev. X **3**, 031010 (2013).
[22] F. Parisen Toldin, M. Hohenadler, F. F. Assaad, and I. F. Herbut, Fermionic quantum criticality in honeycomb and -flux Hubbard models: Finite-size scaling of renormalization-group-invariant observables from quantum Monte Carlo, Phys. Rev. B **91**, 165108 (2015).
[23] Y. Otsuka, S. Yunoki, and S. Sorella, Universal quantum criticality in the metal-insulator transition of two-dimensional interacting Dirac electrons, arXiv:1510.08593.
[24] W. Metzner, Linked-cluster expansion around the atomic limit of the Hubbard model, Phys. Rev. B **43**, 8549 (1991).
[25] S. Pairault, D. Sénéchal, and A.-M. S. Tremblay, Strong-Coupling Expansion for the Hubbard Model, Phys. Rev. Lett. **80**, 5389 (1998).
[26] S. Pairault, D. Sénéchal, and A.-M. S. Tremblay, Strong-coupling perturbation theory of the Hubbard model, Eur. Phys. J. B **16**, 85 (2000).
[27] P. Sahebsara and D. Sénéchal, Hubbard Model on the Triangular Lattice: Spiral Order and Spin Liquid, Phys. Rev. Lett. **100**, 136402 (2008).
[28] A. Yamada, K. Seki, R. Eder, and Y. Ohta, Mott transition and ferrimagnetism in the Hubbard model on the anisotropic kagome lattice, Phys. Rev. B **83**, 195127 (2011).
[29] A. Yamada, K. Seki, R. Eder, and Y. Ohta, Magnetic properties and Mott transition in the square-lattice Hubbard model with frustration, Phys. Rev. B **88**, 075114 (2013).
[30] M. Hafez, S. A. Jafari, and M. R. Abolhassani, Flow equations for the ionic Hubbard model, Phys. Lett. A **373**, 4479 (2009).
[31] M. Hafez, S. A. Jafari, Sh. Adibi, and F. Shahbazi, Classical analog of the ionic Hubbard model, Phys. Rev. B **81**, 245131 (2010).
[32] M. Ebrahimkhas and S. A. Jafari, Short-range Coulomb correlations render massive Dirac fermions massless, Eur. Phys. Lett. **98**, 27009 (2012).
[33] C. Bourbonnais, Ph.D. thesis, Université de Sherbrooke, 1985.
[34] A. Sherman, One-loop approximation for the Hubbard model, Phys. Rev. B **73**, 155105 (2006).
[35] J. P. Hobson and W. A. Nierenberg, The statistics of a two-dimensional, hexagonal net, Phys. Rev. **89**, 662 (1953).
[36] M. Abramowitz and I. A. Stegun, *Handbook of Mathematical Functions with Formulas, Graphs, and Mathematical Tables* (Dover, New York, 1964).
[37] I. F. Herbut, V. Juričić, and O. Vafek, Relativistic Mott criticality in graphene, Phys. Rev. B **80**, 075432 (2009).
[38] B. Rosenstein, H.-L. Yu, and A. Kovner, Critical exponents of new universality classes, Phys. Lett. B **314**, 381 (1993).
[39] L. Janssen and I. F. Herbut, Antiferromagnetic critical point on graphenes honeycomb lattice: A functional renormalization group approach, Phys. Rev. B **89**, 205403 (2014).
[40] T. Horiguchi, Lattice Green's functions for the triangular and honeycomb lattices, J. Math. Phys. **13**, 1411 (1972).